# Improved mechanistic model of the atmospheric redox chemistry of mercury

**Viral Shah[1*], Daniel J. Jacob[1,2], Colin P. Thackray[1], Xuan Wang[3], Elsie M. Sunderland[1,4], Theodore S. Dibble[5], Alfonso Saiz-Lopez[6], Ivan Černušák[7], Vladimir Kellö[7], Pedro J. Castro[5], Rongrong Wu[8], Chuji Wang[8]**

[1] Harvard John A. Paulson School of Engineering and Applied Sciences, Harvard University, Cambridge, MA, USA

[2] Department of Earth and Planetary Sciences, Harvard University, Cambridge, MA, USA

[3] School of Energy and Environment, City University of Hong Kong, Hong Kong SAR, China

[4] Department of Environmental Health, Harvard T.H. Chan School of Public Health, Harvard University, Boston, MA, USA

[5] Department of Chemistry, State University of New York, College of Environmental Science and Forestry, Syracuse, NY, USA

[6] Department of Atmospheric Chemistry and Climate, Institute of Physical Chemistry Rocasolano, CSIC, Madrid, Spain

[7] Department of Physical and Theoretical Chemistry, Faculty of Natural Sciences, Comenius University in Bratislava, Ilkovičova 6, 84215 Bratislava, Slovakia

[8] Department of Physics and Astronomy, Mississippi State University, Starkville, MS, USA

## Abstract

We present a new chemical mechanism for $Hg^0/Hg^I/Hg^{II}$ atmospheric cycling, including recent laboratory and computational data, and implement it in the GEOS-Chem global atmospheric chemistry model for comparison to observations. Our mechanism includes the oxidation of $Hg^0$ by Br atoms and OH radicals, with subsequent oxidation of $Hg^I$ by ozone and radicals, re-speciation of gaseous $Hg^{II}$ in aerosols and cloud droplets, and speciated $Hg^{II}$ photolysis in the gas

and aqueous phases. The tropospheric Hg lifetime against deposition in the model is 5.5 months, consistent with observational constraints. The model reproduces the observed global surface $Hg^0$ concentrations and $Hg^{II}$ wet deposition fluxes. Br and OH make comparable contributions to global net oxidation of $Hg^0$ to $Hg^{II}$. Ozone is the principal $Hg^I$ oxidant, enabling the efficient oxidation of $Hg^0$ to $Hg^{II}$ by OH. $BrHg^{II}OH$ and $Hg^{II}(OH)_2$ are the initial $Hg^{II}$ products of $Hg^0$ oxidation, re-speciate in aerosols and clouds to organic and inorganic complexes, and volatilize to photostable forms. Reduction of $Hg^{II}$ to $Hg^0$ takes place largely through photolysis of aqueous $Hg^{II}$-organic complexes. 71% of model $Hg^{II}$ deposition is to the oceans. Major mechanism uncertainties for atmospheric Hg chemistry modeling include the concentrations of Br atoms, the stability and reactions of $Hg^I$, and the speciation of $Hg^{II}$ in aerosols and clouds with implications for photoreduction.

**Keywords:** mercury modeling, chemical mechanism, mercury oxidation, mercury photoreduction, atmospheric lifetime, mercury deposition

**Synopsis:** Mercury spreads globally through the atmosphere and its atmospheric chemistry determines where it deposits to the surface ecosystems. We present an improved and up-to-date model of atmospheric mercury chemistry.

## Introduction

Mercury (Hg) is an ecosystem pollutant transported globally through the atmosphere. It is emitted in gaseous elemental state ($Hg^0$) by natural and anthropogenic sources, and cycles in the atmosphere with divalent ($Hg^{II}$) compounds that are highly water-soluble and rapidly deposited. Recent theoretical calculations show fast gas-phase reduction of the major $Hg^{II}$ species thought to be produced in the atmosphere,[1–4] posing a challenge for atmospheric models to reproduce the atmospheric Hg concentrations and lifetime inferred from observations.[5] At the same time, new oxidation pathways to form $Hg^{II}$ in the atmosphere have been proposed.[5,6] Here we integrate these recent developments into a new chemical mechanism for atmospheric models to shed new light on the redox cycling of atmospheric Hg.

$Hg^0$ is emitted to the atmosphere by mining, fuel combustion, and volcanism, and by volatilization of previously deposited Hg.[7,8] The $Hg^0$ oxidation pathways and the speciation of $Hg^{II}$ remain highly uncertain.[9–11] The Br atom is considered to be a major $Hg^0$ oxidant.[12–15] The oxidation of $Hg^0$ to $Hg^{II}$ by Br takes place in two steps, beginning with the formation of a $BrHg^I$ intermediate that then undergoes further oxidation to $Hg^{II}$.[16–18] $NO_2$ and $HO_2$ have been thought to be the main $BrHg^I$ oxidants,[19] but the $BrHg^{II}ONO$ and $BrHg^{II}OOH$ products are rapidly photolyzed.[1] Preliminary theoretical calculations by Saiz-Lopez et al.[5] show that $BrHg^I$ may react rapidly with ozone to produce a $BrHg^{II}O$ radical, which can then be stabilized to non-radical $Hg^{II}$ forms by subsequent reactions.[2–4,20]

The oxidation of $Hg^0$ by OH has been included in many models,[21–24] but its atmospheric relevance has been questioned because of the low stability of $HOHg^I$.[17,25] Dibble et al.[6]

recalculated the stability of $HOHg^{I}$ and found the OH-initiated oxidation pathway to be potentially more important than previously thought. Oxidation of $Hg^0$ by ozone[26,27] and BrO[28] has been observed in the laboratory, but is not expected to be atmospherically relevant because the putative product ($Hg^{II}O$) is weakly bound in the gas phase.[29–31] Oxidation of $Hg^0$ by the Cl atom is fast and the $Hg^{I}Cl$ product is tightly bound,[32] but the importance of this pathway is limited by the low Cl atom concentrations in the troposphere.[33,34] Other atmospheric $Hg^0$ oxidation pathways including in aerosols and clouds are thought to be negligible because of either slow rates or low oxidant concentrations.[33]

Partitioning of gas-phase $Hg^{II}$ species into aerosols and cloud droplets adds further complexity to the problem. Atmospheric observations indicate that this partitioning is governed by thermodynamic equilibrium.[35] Once in the condensed phase, $Hg^{II}$ may re-speciate as different inorganic and organic complexes that then partition back to the gas phase.[36] $Hg^{II}Cl_2$ produced in this manner is stable against photolysis and could thus dominate the $Hg^{II}$ pool.[1] $Hg^{II}$-organic complexes photoreduce to $Hg^0$ though not as quickly as some of the inorganic complexes.[1,37]

Although uncertainties in the $Hg^0/Hg^{I}/Hg^{II}$ atmospheric redox cycling remain large, we show here that the most recent laboratory and computational data can be accommodated in a chemical mechanism that reproduces the main features of atmospheric observations and thus provides a basis for Hg modeling. We implement this mechanism in the GEOS-Chem global model, which has been used extensively for the study of atmospheric Hg and its cycling with ocean and land reservoirs.[1–7] Our work represents a major revision to the previous GEOS-Chem mechanism described by Horowitz et al.[33]

## Materials and methods

### Chemical mechanism

Table 1 lists the chemical mechanism and Figure 1 shows the main reaction pathways. $Hg^0$ oxidation is initiated by the radicals $Y \equiv$ Br, Cl, and OH, forming weakly bound intermediates, $YHg^I$, that further add another radical, $Z$, to form $YHg^{II}Z$:

$$Hg^0 + Y + M \leftrightarrow YHg^I + M \quad \text{R1}$$

$$YHg^I + Z + M \rightarrow YHg^{II}Z + M \quad \text{R2}$$

The reaction of $Hg^0$ with Br is exothermic and barrierless,[16,17,43] and its kinetics have been experimentally measured.[44,45] $BrHg^I$ has a low bond energy and dissociates thermally within minutes,[18,19] but its association reactions with $Z \equiv$ OH, Br, $NO_2$, $HO_2$, BrO, ClO are also barrierless and fast.[17,19,46] $BrHg^{II}ONO$ and $BrHg^{II}OOH$ are thought to be the major products due to the abundance of $NO_2$ and $HO_2$.[19,46,47] $BrHg^I$ does not abstract hydrogen atoms and is inefficient in adding to C=C double bonds.[48] It undergoes displacement reactions with certain radicals ($Z_1 \equiv NO_2$ and Br) to return $Hg^0$:[43,46]

$$YHg^I + Z_1 \rightarrow Hg^0 + YZ_1 \quad \text{R3}$$

This chemistry has been included previously in the GEOS-Chem mechanism[33,49] and other models.[50–52] Here we update the rate coefficient for Reaction (R2) based on recent laboratory measurement of the $BrHg^I + NO_2$ reaction.[53]

The OH-initiated oxidation of $Hg^0$ to $Hg^{II}$ also proceeds by the (R1)-(R2) two-step mechanism, and $HOHg^I$ is analogous to $BrHg^I$ in forming thermally stable $HOHg^{II}Z$ ($Z \equiv NO_2$, $HO_2$, etc.) species.[6,17,25] The $Hg^0 + OH + M \rightarrow HOHg^I + M$ reaction is exothermic and fast,[54–56] but theoretical calculations by Goodsite et al.[17] found $HOHg^I$ to be so weakly bound that it would thermally decompose rather than form $Hg^{II}$. As a result, this pathway was discounted in past GEOS-Chem mechanisms.[33,57] However, Dibble et al.[6] found a much higher bond energy for $HOHg^I$ and so we reconsider this pathway here.

Oxidation of $Hg^0$ by Cl atoms is fast[32,44] and $ClHg^I$ is thermally stable, but tropospheric Cl concentrations are low. We include it using GEOS-Chem Cl concentrations from Wang et al.[58] but find that it accounts for less than 1% of global tropospheric $Hg^0$ conversion to $Hg^{II}$. Horowitz et al.[33] included the aqueous-phase oxidation of $Hg^0$ by HOCl, OH, and ozone in cloud droplets but found them to be negligible due to the low solubility of $Hg^0$ and we do not include them in our mechanism.

Standard chemical mechanisms for atmospheric Hg, including Horowitz et al.,[33] do not include gas-phase photoreduction of $Hg^{II}$. However, theoretical calculations indicate that $BrHg^{II}Z$ ($Z \equiv$ $NO_2$, $HO_2$, OH, BrO, ClO) species rapidly photolyze.[1,3] The major $Hg^{II}$ species, $BrHg^{II}ONO$ and $BrHg^{II}OOH$, photolyze on a time scale of minutes.[1,2] $YHg^I$ ($Y \equiv$ Br, Cl, OH) species also photo-dissociate rapidly to $Hg^0$.[59]

Saiz-Lopez et al.[5] found that including $Hg^{I}$ and $Hg^{II}$ photolysis in their global model greatly lowered the net conversion rate of $Hg^{0}$ to $Hg^{II}$ and led to large overestimate of atmospheric $Hg^{0}$ concentrations. Their results implied a missing Hg oxidation pathway in current mechanisms, and they suggested the oxidation of $BrHg^{I}$ by ozone:

$$BrHg^{I} + O_3 \rightarrow BrHg^{II}O + O_2 \qquad \text{R4}$$

Reaction (R4) is strongly exothermic.[60] Theoretical calculations by Saiz-Lopez et al.[5] suggest that it is likely barrierless and produces the $BrHg^{II}O$ radical. Using methods similar to theirs (density functional theory), as well as more advanced CASPT2 calculations, we also find no barrier (Figure S1). Preliminary experimental data indicate a fast reaction consistent with the absence of barrier (Figure S2). We find that the analogous reaction of $HOHg^{I}$ with ozone also lacks a barrier and has similar exothermicity to reaction (R4) (Figure S3), reflecting the similarity between $BrHg^{I}$ and $HOHg^{I}$ (6). Saiz-Lopez et al.[5] estimated an upper limit of $1\times10^{-10}$ $cm^3$ $molec^{-1}$ $s^{-1}$ for the rate coefficient of reaction (R4), assuming no steric effects. Here we estimate a rate coefficient of $3\times10^{-11}$ $cm^3$ $molec^{-1}$ $s^{-1}$ for the reaction of $YHg^{I}$ with ozone ($Y\equiv$ Br, OH, Cl).

The $BrHg^{II}O$ radical is also formed from the photolysis of certain $BrHg^{II}Z$ species (Table 1b). Its reactivity mimics that of OH, and it forms stable $Hg^{II}$ species by abstracting H atoms from methane and other volatile organic compounds, or by associating with NO and $NO_2$, with the methane reaction dominating.[2,20] Khiri et al.[4] found that $BrHg^{II}O$ can also be reduced to $BrHg^{I}$

158 by CO. $BrHg^{II}O$ photolysis in the troposphere is relatively slow.[3] Thus, we include the following
159 reactions in our mechanism:
160
161 $$Y\mathrm{Hg^{I}} + \mathrm{O_3} \rightarrow Y\mathrm{Hg^{II}O} + \mathrm{O_2} \quad \text{R5}$$
162 $$Y\mathrm{Hg^{II}O} + \mathrm{CH_4} \rightarrow Y\mathrm{Hg^{II}OH} + \mathrm{CH_3} \quad \text{R6}$$
163 $$Y\mathrm{Hg^{II}O} + \mathrm{CO} \rightarrow Y\mathrm{Hg^{I}} + \mathrm{CO_2} \quad \text{R7}$$
164
165 $Hg^{II}$ species are absorbed by aqueous aerosol particles and cloud droplets and dissociate to $Hg^{2+}$
166 ions, which re-partition to form inorganic and organic complexes.[36] We refer to total particulate
167 mercury as $Hg^{II}P$. $Hg^{II}Cl_2$, $Hg^{II}Cl_3^-$, and $Hg^{II}Cl_4^{2-}$ are expected to be the dominant inorganic $Hg^{II}$
168 species in the troposphere because of the abundance of $Cl^-$.[61,62] $Hg^{II}$-organic complexes may also
169 form, involving in particular the carboxyl and thiol functional groups.[63,64] In stratospheric
170 sulfuric acid aerosols, $Hg^{II}$ likely remains in free ionic form because of the low stability of the
171 $Hg^{II}$-sulfate complex. While the thermodynamics of the $Hg^{II}$-chloride complexes are known,[36]
172 there is little information on the $Hg^{II}$-organic complexes in atmospheric waters. We choose to
173 represent the inorganic and organic complexes by two species – $Hg^{II}P$(inorg) and $Hg^{II}P$(org) –
174 and partition the dissolved $Hg^{II}$ into these two complexes based on the local relative mass
175 fractions of inorganic and organic aerosol material (Table 1c). Volatilization of $Hg^{II}$ from
176 aerosols is as a parameterized species, $Hg^{II}X$, that is stable against photolysis. We assume for
177 modeling purposes that $Hg^{II}X$ is $Hg^{II}Cl_2$, which does not photolyze at tropospheric wavelengths,[5]
178 but it could include also other stable $Hg^{II}$ species hence the parameterized representation.
179

Photoreduction of $Hg^{II}$ to $Hg^0$ has long been known to occur in atmospheric waters.[65] It was initially thought to involve sulfite ions or $HO_2$ as reductants,[66,67] but it most likely takes place through the direct light absorption by $Hg^{II}$-organic complexes followed by transfer of two electrons from the ligand to Hg.[68,69] $Hg^{II}$ photoreduction is known to involve $Hg^{II}$-organic complexes in aquatic systems.[70–72] Aqueous $Hg^{II}$ photoreduction frequencies of 0.02–0.2 $h^{-1}$ have been measured in summertime rainwater samples,[1] consistent with photoreduction frequencies of $Hg^{II}$-fulvic acid complexes,[37] but lower than 0.2–3 $h^{-1}$ observed in fresh and marine waters.[73] In our mechanism, we assume that the photoreduction frequency of $Hg^{II}P$(org) scales as the local $NO_2$ photolysis frequency ($J_{NO2}$) and adjust the scaling factor ($\beta$ in Table 1b) to fit observed atmospheric $Hg^0$ concentrations. We obtain a scaling factor $\beta = 4\times10^{-3}$, corresponding to a tropospheric mean $Hg^{II}P$(org) photoreduction frequency of 0.13 $h^{-1}$ in clear sky at noon in summer at 45ºN.

## GEOS-Chem model

We implement the chemical mechanism of Table 1 in the global 3-D GEOS-Chem model (www.geos-chem.org; version 12.9.0). The current standard version of the model for Hg is described by Horowitz et al.[33] and includes dynamic coupling between the atmosphere and surface reservoirs. Here we focus on the atmospheric reservoir and therefore use gridded land and ocean surface Hg concentrations from Horowitz et al.[33] as boundary conditions. Other Hg emissions (Figure 1) are also from Horowitz et al.[33] except that anthropogenic Hg emissions are from Streets et al.[74] Total Hg emission in the model is 8.7 Gg $a^{-1}$, of which 0.8 Gg $a^{-1}$ is as $Hg^{II}$ (from combustion) and emitted as $Hg^{II}X$ (Figure 1).

We drive our simulation with assimilated meteorological fields from the NASA Modern-Era Retrospective analysis for Research and Applications, version 2 (MERRA-2) system.[75] We conduct a three-year global simulation (2013–2015) at 4° latitude by 5° longitude resolution following a spin-up period of 15 years to equilibrate the stratosphere. The chemical mechanism is implemented using the Kinetic PreProcessor (KPP)[76] customized for GEOS-Chem, and the chemical evolution is computed every hour on the model grid.

GEOS-Chem in its 'full-chemistry' implementation includes detailed oxidant-aerosol chemistry in the troposphere and stratosphere.[34,77–79] For computational efficiency, the Hg simulation in GEOS-Chem uses monthly oxidant and aerosol concentrations archived from that full-chemistry simulation. Horowitz et al.[33] used Br concentration fields from Schmidt et al.[80] but these are now thought to be too high[81] and do not include the known source of bromine radicals from debromination of sea salt aerosols (SSA).[82] Here we use updated oxidant and aerosol fields from GEOS-Chem version 12.9, including major update of bromine chemistry to include mechanistic SSA debromination and less efficient heterogeneous recycling of bromine radicals.[1] The tropospheric mean Br and BrO concentrations are 0.03 and 0.19 pptv, respectively, compared to 0.08 and 0.48 pptv in Schmidt et al.,[80] but concentrations are higher in the marine boundary layer (MBL) because of SSA debromination (Figure S4). Tropospheric bromine chemistry remains very uncertain,[1] therefore we also conduct a sensitivity simulation using the Schmidt et al.[80] Br and BrO fields. We apply a diurnal scaling to the monthly mean oxidant concentrations using the Y–YO–$O_3$–NO ($Y$≡Br, Cl) photochemical equilibrium for the daytime concentrations of Br, BrO, Cl, ClO following Holmes et al.[57]; a cosine function of the solar zenith angle for daytime

OH and $HO_2$; and NO–$NO_2$–$O_3$ photochemical equilibrium for $NO_2$. Br and BrO concentrations in the polar springtime boundary layer are calculated following Fisher et al.[83]

We treat the transfer of $Hg^{II}$ between the gas phase and the aerosol/cloud phase as a kinetic process. Individual gas-phase species $Hg_i^{II}$ are taken up by aerosols and cloud droplets where they are re-speciated to the $Hg^{II}P$(org) and $Hg^{II}P$(inorg) forms, and then volatilized (for aerosols) as the $Hg^{II}X$ form. The rate of uptake and volatilization of $Hg^{II}$ gaseous species is calculated as:[84,85]

$$-\frac{d[\mathrm{Hg}_i^{\mathrm{II}}(\mathrm{g})]}{dt} = k_{mt}\left[\mathrm{Hg}_i^{\mathrm{II}}(\mathrm{g})\right] \quad (1)$$

$$\frac{d[\mathrm{Hg}^{\mathrm{II}}\mathrm{X}(\mathrm{g})]}{dt} = k_{mt}\,[\mathrm{Hg}^{\mathrm{II}}(\mathrm{g})]_{\mathrm{eq}}\,, \quad (2)$$

where $\left[\mathrm{Hg}_i^{\mathrm{II}}(\mathrm{g})\right]$ is the number density of $\mathrm{Hg}_i^{\mathrm{II}}(\mathrm{g})$, $k_{mt}$ is the mass transfer rate coefficient ($s^{-1}$), and $[\mathrm{Hg}^{\mathrm{II}}(\mathrm{g})]_{\mathrm{eq}}$ is calculated on the basis of equilibrium between total $Hg^{II}$ in the gas and aerosol phases using the empirical equilibrium constant of Amos et al.[35] as a function of local temperature and mass concentration of fine particulate matter. For cloud droplets, we assume no mass transfer back to the gas phase because of the high solubility of $Hg^{II}$. Uptake on coarse-mode SSA follows Holmes et al.[57] $k_{mt}$ for aerosols is calculated as:

$$k_{mt} = \sum_j S_j \left(\frac{r_j}{D_g} + \frac{4}{\nu\alpha}\right)^{-1}, \quad (3)$$

where $r_j$ and $S_j$ are the effective mean area-weighted radius and surface area per unit volume of air of each aerosol component ($j$), $D_g$ is the gas-phase molecular diffusion coefficient of $Hg^{II}$ gas, $v$ is the mean molecular speed of $Hg^{II}$ gas, and $\alpha$ is the mass accommodation coefficient. We take $\alpha = 0.1$ for all $Hg^{II}$ gas species in the model since $\alpha$ for other highly soluble species generally has values of 0.1–0.3.[86] $k_{mt}$ for cloud droplets is calculated similarly but also accounts for entrainment limitation in partly cloudy grid cells.[87]

## Results and discussion

### Global atmospheric Hg budget

Figure 1 shows the global model Hg budget for the troposphere and the major pathways for $Hg^0$/$Hg^I$/$Hg^{II}$ redox cycling. The tropospheric mass of Hg is 4 Gg (3.9 Gg as $Hg^0$ and 0.1 Gg as $Hg^{II}$). The stratosphere contains an additional 0.8 Gg (not shown in Fig. 1). The tropospheric lifetime of total Hg ($Hg^0$+$Hg^I$+$Hg^{II}$) against deposition is 5.5 months. The simulated Hg mass and lifetime are within observationally constrained values of ~4 Gg for the tropospheric Hg mass and 4–7 months for the Hg lifetime.[5,23,33,57] The previous GEOS-Chem simulation of Horowitz et al.[33] had a tropospheric mass of Hg of 3.9 Gg and a lifetime against deposition of 5.2 months, similar to ours, but four times as much $Hg^{II}$ (0.4 Gg) because of production at higher altitudes (leading to longer lifetime against deposition) and slower photoreduction.

We find that oxidation of $Hg^0$ to $Hg^I$ takes place by Br and OH at similar rates. Ozone is the primary oxidant of $Hg^I$ to $Hg^{II}$ as it is far more abundant than $NO_2$ and $HO_2$, which were the main $Hg^I$ oxidants in previous mechanisms.[1,5,33] The inclusion of ozone as an oxidant for $HOHg^I$ allows OH to contribute extensively to net $Hg^0$ oxidation outside of the urban boundary layer

(compare Dibble, et al. 2019). Photolysis and thermal decomposition of $BrHg^{I}$ are much slower than its reaction with ozone, so the main fate of $BrHg^{I}$ is oxidation to $BrHg^{II}OH$, via $BrHg^{II}O$. Although $HOHg^{I}$ is less stable than $BrHg^{I}$ and a smaller fraction of it is converted to $Hg^{II}$, the OH-initiated pathway still accounts for one-third of the global $Hg^{II}$ production. The chemical lifetime of $Hg^{0}$ against oxidation to $Hg^{II}$ in our model is 4.5 months, compared to 2.7 months in Horowitz et al.[33] and about 13 months in Saiz-Lopez et al.[1] Using higher free tropospheric Br concentrations from Schmidt et al.[80] lowers the tropospheric Hg mass by about 10% due to increased partitioning to $Hg^{II}$ and hence faster deposition. Br then contributes 75% of $Hg^{0}$ oxidation (Figure S5).

Figure 2 shows the zonal distribution of the $Hg^{0}$ oxidation rate in our standard simulation. Gross oxidation of $Hg^{0}$ to $Hg^{II}$ is fastest in the MBL and in the upper troposphere and largely reflects the Br distribution. Br concentrations are highest near the tropical tropopause due to fast photolysis of BrO and low ozone and temperature.[88,89] The OH-initiated oxidation pathway contributes most to $Hg^{0}$ oxidation in the tropical free troposphere, as dissociation of $HOHg^{I}$ is fast at lower altitudes.[6] It also dominates in the continental boundary layer, consistent with Gabay et al.,[90] because Br concentrations are low there.

$BrHg^{II}OH$ and $Hg^{II}(OH)_2$ are the main $Hg^{II}$ species initially formed from $Hg^{0}$ oxidation, but the $Hg^{II}$ speciation evolves as these species are processed by aerosol and cloud droplets to form $Hg^{II}P$ particles and $Hg^{II}X$ gas. We find that $Hg^{II}X$ (modeled as $Hg^{II}Cl_2$) is the most abundant form of $Hg^{II}$ in the troposphere, comprising 49% of $Hg^{II}$ mass, while $Hg^{II}P$ comprises 22%. The remaining $Hg^{II}$ mass is mostly composed of $Hg^{II}(OH)_2$, which is more abundant than $BrHg^{II}OH$

because it does not photolyze. Most of the reduction of $Hg^{II}$ to $Hg^0$ is through the aqueous-phase photolysis of $Hg^{II}P$(org). The photoreduction rate increases with altitude because of stronger UV radiation and the higher $Hg^{II}$ particle fraction at lower temperatures, and it is faster in the northern hemisphere because of the higher fraction of organic aerosol. $Hg^{II}P$ is stable against photoreduction in the stratosphere as it is assumed to be present as free $Hg^{2+}$.

The net rate of oxidation of $Hg^0$ to $Hg^{II}$, accounting for $Hg^{II}$ reduction, is 43% of the gross $Hg^0$ oxidation rate. Net $Hg^0$ oxidation is fastest in the MBL where $Hg^{II}$ photoreduction is slower than deposition. Horowitz et al.[33] found little net oxidation in the lower troposphere because their simulation had little Br in the MBL and did not include the $Hg^I + O_3$ reaction. They had maximum production in the tropical upper troposphere, but here this is largely canceled by photoreduction and we find areas of net reduction as the $Hg^{II}$-rich tropical upper tropospheric air is transported poleward by the Hadley circulation. Globally, we find that about half of the net oxidation of $Hg^0$ to $Hg^{II}$ takes place through the OH-initiated pathway, compared to one-third for gross oxidation, because of the stability of $Hg^{II}(OH)_2$ against photolysis.

Our results differ substantially from the global model simulation of Saiz-Lopez et al.[5] They found that including the photolysis of $Hg^I$ and $Hg^{II}$ species increased the Hg lifetime against deposition to 20 months and the tropospheric Hg mass to 7.9 Gg, twice higher than inferred from atmospheric observations. Including the $BrHg^I+O_3$ reaction lowered the tropospheric Hg lifetime to 15 months, which is still too high. The Hg lifetime in their model would have been even longer had they included the recent findings on the reduction of $BrHg^{II}O$ by CO,[4] and the slower $BrHg^I+NO_2$ rate coefficient.[53] The main reasons why we achieve a shorter Hg lifetime are

because we include (1) the $HOHg^{I}+O_3$ reaction, which accounts for half of the net chemical loss of $Hg^0$ in our model; and (2) the re-speciation of photolabile $Hg^{II}$ species in aerosols and cloud droplets to form more stable species.

## Spatial distribution of Hg concentrations and deposition

Figure 3 shows the modeled zonal distributions of $Hg^0$ and $Hg^{II}$ concentrations and compares modeled and observed $Hg^0$ concentrations at the surface. There is little variation in $Hg^0$ concentrations with altitude in the troposphere, both in the model and in aircraft measurements,[91–93] consistent with the long lifetime of $Hg^0$. Modeled $Hg^0$ concentrations decrease by ~50 ppq within a height of 3 km above the tropopause, which is somewhat lower than the decrease (~70 ppq) observed from aircraft,[93] This could reflect excessive mixing across the tropopause in the 4°×5° version of the model.[94] The model captures the observed spatial patterns in surface $Hg^0$ concentrations ($r$ = 0.86), which are driven by anthropogenic emissions and the interhemispheric gradient, but it underestimates the observed variability. The model overestimates the observed $Hg^0$ concentrations in the southern hemisphere by about 20 ppq but this could reflect uncertainty in ocean $Hg^0$ emissions.[33]

Figure S6 compares the simulated and observed $Hg^0$ concentrations in surface air for different latitudinal bands. Polar concentrations show a spring minimum both in the observations and in the model due to high bromine in the polar MBL.[1,2] Observations at northern midlatitudes show minimum concentrations in summer-fall, previously attributed in GEOS-Chem to oxidation by OH and Br,[1,2] but here the model minimum is shifted to spring because of the large Br source from SSA debromination.[1] There is no significant seasonal variation in the tropics either in the

338 model or in the observations. Observations at southern mid-latitudes also show no significant
339 seasonal variation but the model has a summer minimum driven by $Hg^0$ oxidation. Interpretation
340 of model errors in reproducing the observed $Hg^0$ seasonal variations is complicated by
341 uncertainties in the seasonality of ocean and land fluxes.[1]
342
343 Simulated $Hg^{II}$ concentrations increase with altitude in the troposphere – from 1 ppq in surface
344 air to 15 ppq at the tropopause – reflecting the sink from deposition. Concentrations are highest
345 in the subtropics due to subsidence of $Hg^{II}$ produced in the tropical upper troposphere.[95,96]
346 Values in surface air are consistent with long-term $Hg^{II}$ observations made using KCl-coated
347 denuders (Figure S7), but these measurements are known to be biased low.[97,98] Aircraft
348 measurements find an average of 10 ppq $Hg^{II}$ in the free troposphere at northern midlatitudes,[5]
349 much higher than in the model (Figure 3). Using the higher Br concentrations from Schmidt et
350 al.[80] in the model does not fix the problem, but slower aqueous photoreduction would. We
351 conducted a sensitivity simulation in which aqueous $Hg^{II}$ photoreduction was limited to liquid
352 cloud droplets and $Hg^{II}P$(org) formation on aerosol particles was excluded, similar to Saiz-Lopez
353 et al.,[1,5] and found a doubling of $Hg^{II}$ concentrations in the free troposphere. However,
354 $Hg^{II}P$(org) photoreduction frequency in cloud droplets required to fit the observed Hg lifetime
355 against deposition in that sensitivity simulation was much higher and inconsistent with the
356 rainwater observations of Saiz-Lopez et al.[1]
357
358 Figure 4 shows the observed and modeled $Hg^{II}$ wet deposition fluxes, as well as the modeled
359 total (wet + dry) $Hg^{II}$ deposition flux. The mean Hg wet deposition flux for the global ensemble
360 of sites is 25% lower in the model than in the observations. The model shows maximum wet

deposition flux over eastern China because of high anthropogenic $Hg^{II}$ emissions, but this is not seen in observations, suggesting that China's $Hg^{II}$ emissions may be overestimated due to insufficient accounting of recent emission controls.[99] The model captures the regional maximum of $Hg^{II}$ wet deposition over the Southeast US driven by deep convective scavenging of free tropospheric $Hg^{II}$-rich air[100–102], but underestimates its magnitude because of the previously discussed underestimate of $Hg^{II}$ in the free troposphere.

The global $Hg^{II}$ wet deposition flux in our standard simulation is 2.6 Gg $a^{-1}$ and the total (wet + dry) $Hg^{II}$ deposition flux is 5.5 Gg $a^{-1}$. Another 1.2 Gg $a^{-1}$ is dry deposited to land as $Hg^0$. We find that 71% of $Hg^{II}$ deposition takes place over the oceans, where it is the main source of Hg for the marine biosphere,[103,104] and is 15% higher in the northern than in the southern hemisphere. Horowitz et al.[33] found a higher fraction (82%) of $Hg^{II}$ deposition over the oceans because of faster $Hg^{II}$ reduction over land driven by high organic aerosol. Holmes et al.[57] found that 72% of the $Hg^{II}$ deposition takes place over the oceans, but with a higher flux in the southern hemisphere than in the northern hemisphere, reflecting the Br distribution in their simulation. $Hg^{II}$ deposition over land in our simulation is concentrated largely in $Hg^{II}$ emission hotspots over China, India, and South Africa. Outside of these hotspots, $Hg^0$ dry deposition is the major route for Hg deposition over land, contributing 45% globally, but lower than observational estimates of 50–90%.[105,106]

## Uncertainties in atmospheric Hg redox chemistry

We have aimed to provide a mechanistic representation of Hg redox cycling in the atmosphere that reflects current chemical knowledge while being consistent with fundamental observational

384 constraints. This involved a number of assumptions and here we examine the most
385 consequential.
386
387 An important uncertainty is the oxidation rate of $Hg^0$ by Br, reflecting both the reaction rate
388 coefficient and the Br concentrations. Laboratory determinations of the $Hg^0$+Br rate coefficient
389 vary from $3.6\times10^{-13}$ to $3.2\times10^{-12}$ $cm^3$ $molec^{-1}$ $s^{-1}$ (at 298 K, 1 atm).[44,45,107] We use the rate
390 coefficient from Donohoue et al.,[45] which is at the low end, because their measurements are least
391 affected by wall reactions and were made over a range of pressures and temperatures. Using a
392 higher value would require slower conversion of $BrHg^I$ to $Hg^{II}$, faster $Hg^{II}$ reduction, and/or
393 lower Br concentrations to maintain the same Hg lifetime against deposition in the model. The
394 $BrHg^I \rightarrow Hg^{II}$ rate can be slowed by lowering the $BrHg^I+O_3$ and increasing the $BrHg^IO+CO$ rate
395 coefficients, and while the changes needed are substantial (factor of 10) since the competing
396 $BrHg^I \rightarrow Hg^0$ reactions are currently negligible, they would be within the uncertainties of the
397 theoretically derived rate coefficients.[108] Faster $Hg^{II}$ reduction would still need to fit the observed
398 rainwater photoreduction rates.[1,37] Faster $Hg^0$+Br kinetics could be offset by lower Br
399 concentrations, but the concentrations used here are at the low end of current models as
400 discussed by Wang et al.[34,58]
401
402 The atmospheric OH concentrations are well known[109] and the $Hg^0$+OH rate coefficient agrees
403 between two independent laboratory studies,[54,55] although the pressure and temperature
404 dependences of the rate coefficient need to be further investigated. There are large uncertainties
405 in the $HOHg^I$+M, $HOHg^I+O_3$, $HOHg^{II}O$+CO, and $HOHg^{II}O+CH_4$ reactions that control the
406 branching between $HOHg^I \rightarrow Hg^0$ and $HOHg^I \rightarrow Hg^{II}(OH)_2$. The $HOHg^I$+M rate coefficient

depends on the HO–$Hg^{I}$ bond strength, which has not been determined experimentally.[6] A moderate change in this rate coefficient could be balanced by proportional changes in the rate coefficients of the other three reactions. Slower dissociation of $HOHg^{I}$ (stronger bond) would increase net $Hg^{0}$ oxidation in the subtropical free troposphere and help improve the simulation of the observed Hg wet deposition flux maximum over the Southeast US.

An important part of our mechanism is the photoreduction of $Hg^{II}$ organic complexes in aerosols but there are no direct data to inform the photoreduction rates. Here we have assumed similarity with photoreduction in cloud droplets, which is informed (though weakly so) by the rainwater photoreduction data.[1,35] Dissolved organic carbon is known to be critical for $Hg^{II}$ photoreduction in aquatic systems,[70–72] but there is no knowledge of the relevant organic ligands for atmospheric $Hg^{II}$. A better understanding of particulate and cloud $Hg^{II}$ speciation, and the implications for photoreduction, would greatly advance our modeling capability.

## ASSOCIATED CONTENT

### Supporting Information

Energy profiles for the $BrHg^{I}+O_3$ reaction (Figure S1); Preliminary rate coefficient for $BrHg^{I}+O_3$ as a function of temperature (Figure S2); Potential energy surface for the $HOHg^{I}+O_3$ reaction (Figure S3); Comparison of the zonal mean Br and BrO concentrations in GEOS-Chem version 12.9 and from Schmidt et al. (Figure S4); Main Hg redox pathways and the zonal distribution of $Hg^0$ and $Hg^{II}$ in the simulation with the Schmidt et al. Br concentration (Figure S5); Observed and modeled seasonal variation of surface $Hg^0$ (Figure S6); and Observed and modeled annual surface $Hg^{II}$ concentrations (Figure S7).

## AUTHOR INFORMATION


### Corresponding Author

**Viral Shah:** Harvard John A. Paulson School of Engineering and Applied Sciences, Harvard University, Cambridge, MA 02138, USA

Email: vshah@seas.harvard.edu

### Author information

**Daniel J. Jacob:** Harvard John A. Paulson School of Engineering and Applied Sciences and Department of Earth and Planetary Sciences, Harvard University, Cambridge, MA 02138, USA

**Colin P. Thackray:** Harvard John A. Paulson School of Engineering and Applied Sciences, Harvard University, Cambridge, MA 02138, USA

**Xuan Wang:** School of Energy and Environment, City University of Hong Kong, Hong Kong SAR, China

**Elsie M. Sunderland:** Harvard John A. Paulson School of Engineering and Applied Sciences, Harvard University, Cambridge, MA 02138, USA and Department of Environmental Health, Harvard T.H. Chan School of Public Health, Harvard University, Boston, MA 02115, USA

**Theodore S. Dibble:** Department of Chemistry, State University of New York, College of Environmental Science and Forestry, Syracuse, NY 13210, USA

**Alfonso Saiz-Lopez:** Department of Atmospheric Chemistry and Climate, Institute of Physical Chemistry Rocasolano, CSIC, 28006 Madrid, Spain

**Ivan Černušák:** Department of Physical and Theoretical Chemistry, Faculty of Natural Sciences, Comenius University in Bratislava, Ilkovičova 6, 84215 Bratislava, Slovakia

**Vladimir Kellö:** Department of Physical and Theoretical Chemistry, Faculty of Natural Sciences, Comenius University in Bratislava, Ilkovičova 6, 84215 Bratislava, Slovakia

**Pedro J. Castro:** Department of Chemistry, State University of New York, College of Environmental Science and Forestry, Syracuse, NY 13210, USA

**Rongrong Wu:** Department of Physics and Astronomy, Mississippi State University, Starkville, MS 39762, USA

**Chuji Wang:** Department of Physics and Astronomy, Mississippi State University, Starkville, MS 39762, USA

## Author Contributions

V.S. and D.J.J. developed the chemical mechanism with input from C.P.T., E.M.S., T.S.D., and A.S.-L.; V.S. and C.P.T. implemented the mechanism in GEOS-Chem; X.W. developed the current GEOS-Chem halogen simulation; T.S.D, I.Č, V.K, and P.J.C. performed the quantum chemistry calculations for the reactions of BrHg and HOHg with ozone; R.W. and C.W. conducted laboratory experiments on the BrHg and ozone reaction; V.S. and D.J.J. wrote the manuscript with contributions from all coauthors.

## ACKNOWLEDGMENTS

This work was funded by the US EPA Science to Achieve Results (STAR) Program. This work was also supported by the Slovak Grant Agency VEGA (grant 1/0777/19), the high-performance computing facility of the Centre for Information Technology (https://uniba.sk/en/HPC-Clara) at Comenius University, and the US National Science Foundation under awards 1609848 and 2004100. We thank Hélène Angot (CU Boulder) for the surface measurement data.

## REFERENCES

Automatic citation updates are disabled. To see the bibliography, click Refresh in the Zotero tab.

475 **Table 1a. Chemical mechanism: bimolecular and three-body reactions**

| Reaction | Rate coefficients [a] | References [b] |
|---|---|---|
| $Hg^0 + Br + M \rightarrow BrHg^I + M$ | $k_0 = 1.46 \times 10^{-32} (T/298)^{-1.86}$ | (1) |
| $BrHg^I + M \rightarrow Hg^0 + Br + M$ | $k_0/K_{eq}$; $K_{eq} = 9.14 \times 10^{-24} \exp(7801/T)$ | (2) |
| $Hg^0 + OH + M \rightarrow HOHg^I + M$ | $k_0 = 3.34 \times 10^{-33} \exp(43/T)$ | (3) [c] |
| $HOHg^I + M \rightarrow Hg^0 + OH + M$ | $k_0/K_{eq}$; $K_{eq} = 2.74 \times 10^{-24} \exp(5770/T)$ | (4) |
| $Hg^0 + Cl + M \rightarrow ClHg^I + M$ | $k_0 = 2.25 \times 10^{-33} \exp(680/T)$ | (5) |
| $YHg^I + O_3 \rightarrow YHg^{II}O + O_2$ ($Y \equiv$ Br, OH, Cl) | $3.0 \times 10^{-11}$ | (6) [d, e] |
| $YHg^{II}O + CH_4 \rightarrow YHg^{II}OH + CH_3$ ($Y \equiv$ Br, OH, Cl) | $4.1 \times 10^{-12} \exp(-856/T)$ | (7) [e] |
| $YHg^{II}O + CO \rightarrow YHg^I + CO_2$ ($Y \equiv$ Br, OH, Cl) | $6.0 \times 10^{-11} \exp(-550/T)$ | (8) [e, f] |
| $YHg^I + NO_2 + M \rightarrow YHg^{II}ONO + M$ ($Y \equiv$ Br, OH, Cl) | $k_0 = 4.3 \times 10^{-30} (T/298)^{-5.9}$<br>$k_\infty = 1.2 \times 10^{-10} (T/298)^{-1.9}$ | (9, 10) [e] |
| $YHg^I + Z + M \rightarrow YHg^{II}Z + M$ ($Y \equiv$ Br, OH, Cl; $Z \equiv HO_2$, BrO, ClO) | $k_0 = 4.3 \times 10^{-30} (T/298)^{-5.9}$<br>$k_\infty = 6.9 \times 10^{-11} (T/298)^{-2.4}$ | (9, 10) [e, g] |
| $YHg^I + Z (+ M) \rightarrow YHg^{II}Z (+ M)$ ($Y \equiv$ Br, OH, Cl; $Z \equiv$ Br, Cl, OH) | $3.0 \times 10^{-11}$ | (11) [e, h] |
| $YHg^I + NO_2 \rightarrow Hg^0 + YNO_2$ ($Y \equiv$ Br, Cl) | $3.0 \times 10^{-12}$ | (9) [e] |
| $BrHg^I + Br \rightarrow Hg^0 + Br_2$ | $3.9 \times 10^{-11}$ | (11) |
| $ClHg^I + Cl \rightarrow Hg^0 + Cl_2$ | $1.2 \times 10^{-11} \exp(-5942/T)$ | (12) |

476

477 a. The rate coefficients have units of $cm^3$ $molec^{-1}$ $s^{-1}$ for bimolecular reactions and $cm^6$ $molec^{-2}$ $s^{-1}$ for $k_0$ of
478 three-body reactions. The second-order rate coefficient for three-body reactions is calculated as: $k([M]) =$
479 $\left(\frac{k_0[M]}{1+k_0[M]/k_\infty}\right) 0.6^p$, where $[M]$ is the number density of air molecules and $p = (1 +$
480 $(\log_{10}(k_0[M]/k_\infty))^2)^{-1}$. Only $k_0$ is given when the low-pressure limit dominates in the atmosphere and
481 the second-order rate coefficient is then calculated as $k_0[M]$. For thermal dissociation reactions, the rate
482 coefficient is calculated as $k = k_0/K_{eq}$ where $k_0$ is the rate coefficient of the forward (association) reaction
483 given in the preceding entry and $K_{eq}$ is the equilibrium constant in units of $cm^3$ $molec^{-1}$. $T$ is absolute
484 temperature in K.
485
486 b. (1) Donohoue et al.[45]; (2) Dibble et al.[19]; (3) Pal and Ariya[55]; (4) Dibble et al.[6]; (5) Donohoue et al.[32]; (6)
487 Saiz-Lopez et al.[5]; (7) Lam et al.[2]; (8) Khiri et al.[4]; (9) Wu et al.[53]; (10) Jiao & Dibble[46]; (11) Balabanov et
488 al.[43]; (12) Wilcox[110].
489
490 c. The rate coefficient was calculated by Dibble et al.[6] from the experimental results of Pal and Ariya[55].
491

d. Saiz-Lopez et al.[5] estimated an upper limit for the rate coefficient of $1.0 \times 10^{-10}$ $cm^3$ $molec^{-1}$ $s^{-1}$, assuming no steric effects.

e. We assume that the $BrHg^I + Z$ rate coefficients hold for $HOHg^I + Z$ and $ClHg^I + Z$ because of the similar bond energies and reactions pathways for the three species,[6,19] and that the $BrHg^{II}O+Z$ rate coefficients hold for $HOHg^{II}O+Z$ and $ClHg^{II}O+Z$.

f. Khiri et al.[4] calculated the range for the rate coefficient of the $BrHg^{II}O+CO \rightarrow BrHg^{I}+CO_2$ reaction at two temperatures: $(9.4–52)\times10^{-12}$ $cm^3$ $molec^{-1}$ $s^{-1}$ at 298K and $(3.8–29)\times10^{-12}$ $cm^3$ $molec^{-1}$ $s^{-1}$ at 220K. We use the mean values at each temperature to determine the temperature-dependent rate coefficient.

g. We assume that the experimentally determined value of $k_0$ for the $BrHg^I + NO_2$ reaction[53] holds for this set of reactions too.

h. These reactions take place at the high-pressure limit in the atmosphere and the rate coefficient is given for the effective bimolecular reactions.

**Table 1b. Chemical mechanism: photolysis reactions [a]**

| Reaction | $\phi$ | $J$ ($s^{-1}$) [b] | References [c] |
|---|---|---|---|
| $BrHg^{I} + h\nu \rightarrow Hg^{0} + Br$ | 1.0 | $4.3\times10^{-2}$ | (1) |
| $HOHg^{I} + h\nu \rightarrow Hg^{0} + OH$ | 1.0 | $1.6\times10^{-2}$ | (1) |
| $YHg^{II}OH + h\nu \rightarrow Hg^{0} + Y + OH$<br>$\rightarrow HOHg^{I} + Y$<br>$\rightarrow YHg^{I} + OH$<br>$\rightarrow YHg^{II}O + H$<br>($Y \equiv$ Br, Cl) | 0.49<br>0.35<br>0.15<br>0.01 | $1.3\times10^{-5}$ | (2, 3, 4) [d] |
| $YHg^{II}ONO + h\nu \rightarrow YHg^{II}O + NO$<br>$\rightarrow YHg^{I} + NO_2$<br>($Y \equiv$ Br, Cl, OH) | 0.90<br>0.10 | $1.1\times10^{-3}$ | (2, 3, 4, 5) [d,e] |
| $YHg^{II}OOH + h\nu \rightarrow Hg^{0} + Y + HO_2$<br>$\rightarrow YHg^{II}O + OH$<br>$\rightarrow YHg^{I} + HO_2$<br>($Y \equiv$ Br, Cl, OH) | 0.66<br>0.31<br>0.03 | $1.5\times10^{-2}$ | (2, 3, 4) [d,e] |
| $YHg^{II}OBr + h\nu \rightarrow YHg^{I} + BrO$<br>($Y \equiv$ Br, OH, Cl) | 1.0 [f] | $2.4\times10^{-2}$ | (2) [e] |
| $YHg^{II}OCl + h\nu \rightarrow YHg^{I} + ClO$<br>($Y \equiv$ Br, OH, Cl) | 1.0 [f] | $1.4\times10^{-2}$ | (2) [e] |
| $Hg^{II}Br_2 + h\nu \rightarrow BrHg^{I} + Br$<br>$\rightarrow Hg^{0} + 2Br$ | 0.60<br>0.40 | $1.2\times10^{-6}$ | (2, 4) [d] |
| $Hg^{II}P(org) + h\nu \rightarrow Hg^{0}$ | 1.0 | $1.9\times10^{-5}$ | this work [g] |

a. Photolysis frequencies are calculated using Fast-JX v7.0a[111] implemented in GEOS-Chem by Eastham et al.[77] $\phi$ represents the branching fractions for the dissociation channels. $Hg^{II}(OH)_2$ and $Hg^{II}Cl_2$ are not shown in the table because they do not photolyze at tropospheric wavelengths.[1,112]

b. Global annual mean tropospheric photolysis frequencies in GEOS-Chem.

c. (1) Saiz-Lopez et al.[59]; (2) Saiz-Lopez et al.[1]; (3) Francés-Monerris et al.[3]; (4) Saiz-Lopez et al.[5]; (5) Lam et al.[2]

d. Photolysis cross-sections are from Saiz-Lopez et al.[5] and branching fractions from Francés-Monerris et al.[3] and Saiz-Lopez et al.[5]

e. Photolysis cross-sections for $HOHg^{II}Z$ and $ClHg^{II}Z$ (Z=$NO_2$, $HO_2$, BrO, and ClO) are assumed to be same as for $BrHg^{II}Z$.

f. Sole photolysis pathway considered in Saiz-Lopez et al.[1]

g. The photolysis frequency of this reaction is parameterized as $J_{HgIIP(org)} = \beta J_{NO2}$, where $J_{NO2}$ is the local photolysis frequency of $NO_2$ and the scaling factor $\beta$ is adjusted to match the global mean $Hg^0$ surface observations. For our standard simulation we use $\beta = 4\times10^{-3}$, and for the sensitivity simulation with the Schmidt et al.[80] Br fields we use $\beta = 4\times10^{-2}$.

**Table 1c. Chemical mechanism: multiphase processes**

| Reaction[a] | Notes |
|---|---|
| $Hg^{II}\,(g) \xrightarrow{\text{aerosols,clouds}} Hg^{II}P$ | b |
| $Hg^{II}P \xrightarrow{\text{aerosols}} Hg^{II}X\,(g)$ | c |
| $Hg^{II}P \equiv \begin{cases} Hg^{II}P(org) + Hg^{II}P(inorg) & \text{(troposphere)} \\ Hg^{2+} & \text{(stratosphere)} \end{cases}$ | d |

a. $Hg^{II}$ (g) and $Hg^{II}P$ represent all gas- and particle-phase $Hg^{II}$ species; $Hg^{II}X$ (g) represents the unspeciated $Hg^{II}$ gas volatilizing from $Hg^{II}P$ and treated as $Hg^{II}Cl_2$.

b. $Hg^{II}$(g) uptake rate is given by Eq (1). For clouds, the uptake rate accounts for entrainment limitation in partly cloudy grid cells.[87]

c. Volatilization is considered only for tropospheric aerosols, not for cloud droplets (because of their large volume) and stratospheric aerosols (because of their high acidity and cold temperature). The volatilization rate is given by Eq (2) with equilibrium constant between $Hg^{II}$(g) and $Hg^{II}P$ from Amos et al.[35]

d. $Hg^{II}P$ in the tropospheric aerosol speciates as $Hg^{II}P$(org) and $Hg^{II}P$(inorg) representing $Hg^{II}$-organic and $Hg^{II}$-inorganic complexes. Their concentrations are calculated as $[Hg^{II}P(org)] = f_{OA}[Hg^{II}P]$ and $[Hg^{II}P(inorg)] = (1 - f_{OA})[Hg^{II}P]$, where $f_{OA}$ is the local mass fraction of organic aerosols in fine particles computed as $f_{OA} = \frac{m_{OA}}{m_{OA}+m_{IA}}$, with $m_{OA}$, and $m_{IA}$ representing the respective mass concentrations of organic and inorganic aerosol components.

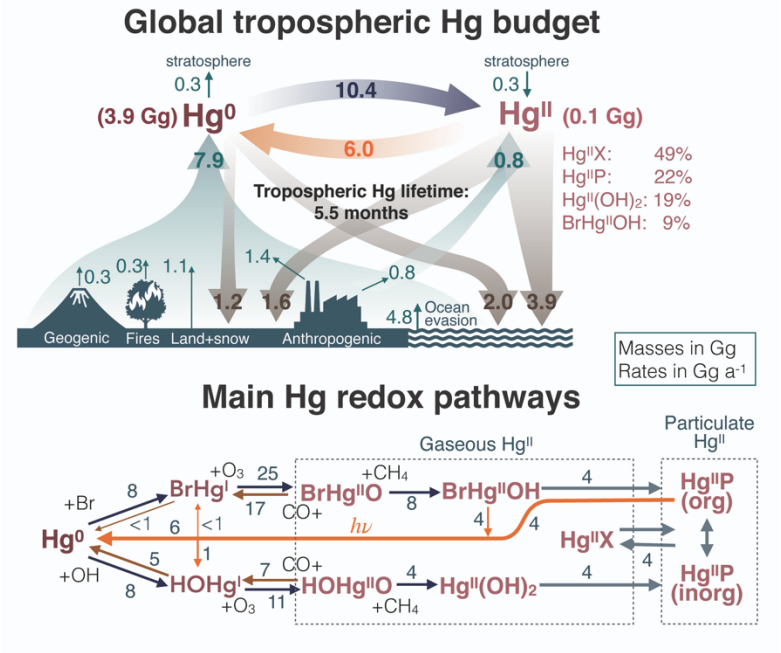


**Figure 1. Global tropospheric Hg budget and main Hg redox pathways in our simulation for 2013–2015. The Hg masses and rates are global annual means given in units of Gg and Gg $a^{-1}$ respectively. The tropospheric mass of $Hg^{I}$ is very small ($3\times10^{-6}$ Gg) and not shown. The main $Hg^{II}$ species in the model and their percent contributions to the total tropospheric $Hg^{II}$ mass are listed. $Hg^{II}P$ denotes particulate $Hg^{II}$, which includes $Hg^{II}$-organic complexes ($Hg^{II}P$(org)), and $Hg^{II}$-inorganic complexes ($Hg^{II}P$(inorg)). $Hg^{II}X$ denotes the gas-phase $Hg^{II}$ species that volatilize from $Hg^{II}P$ and is modeled as $HgCl_2$. Oxidation of $Hg^0$ by Cl atoms is not shown because it accounts only for <1% of the $Hg^0$ chemical sink in the troposphere.**

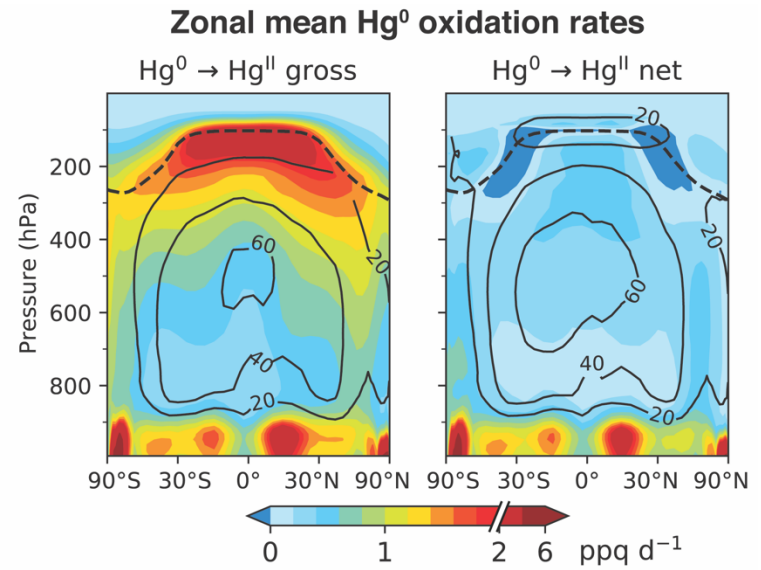


**Figure 2. Annual (2013–2015) zonal mean gross and net $Hg^0$ oxidation rates in GEOS-Chem. The contour lines show the percent contribution of the OH-initiated $Hg^0$ oxidation pathway. The dashed line denotes the annual-mean tropopause.**

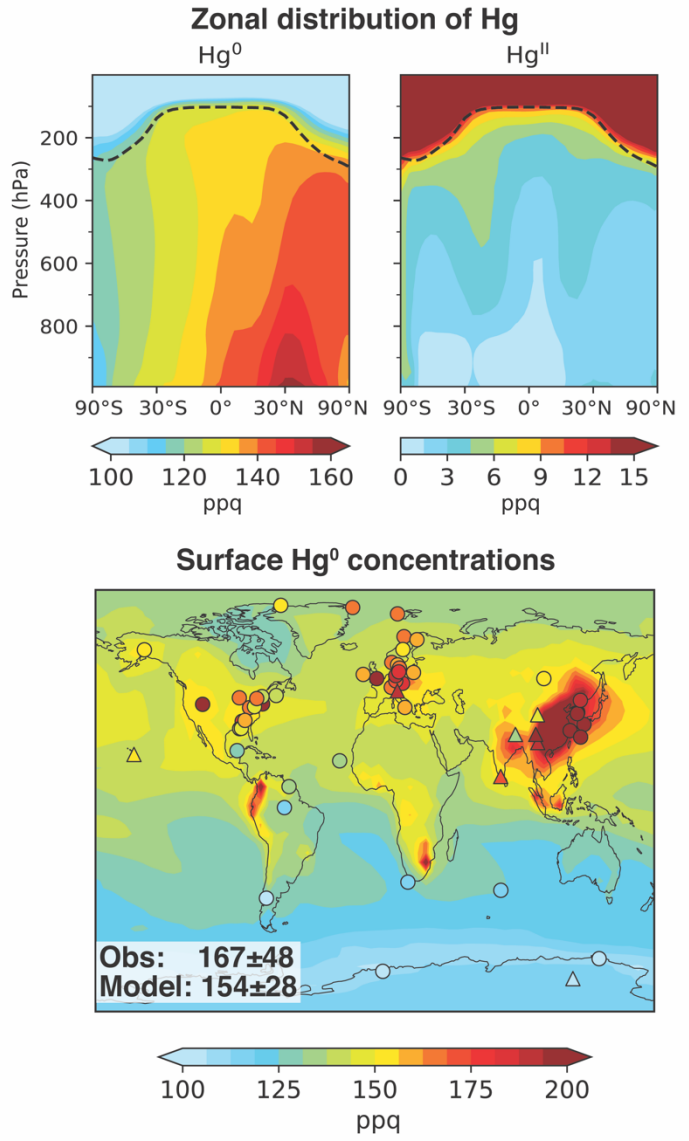


**Figure 3. Annual mean (2013–2015) concentrations of $Hg^0$ and $Hg^{II}$ in GEOS-Chem. The top panels are zonal mean concentrations as a function of pressure and sine latitude. The dashed lines indicate the annual mean tropopause. The bottom panel compares the modeled surface $Hg^0$ concentrations with observations (filled circles and triangles) from the compilations of Travnikov et al.[51] (courtesy of Hélène Angot) and AMAP/UNEP.[113] Filled triangles represent high altitude sites. We only include observations made between 2010 and 2015. The mean ± standard deviation of the observed concentrations is inset in the bottom panel along with the corresponding model values sampled at the site locations. The color scales are different for each panel.**

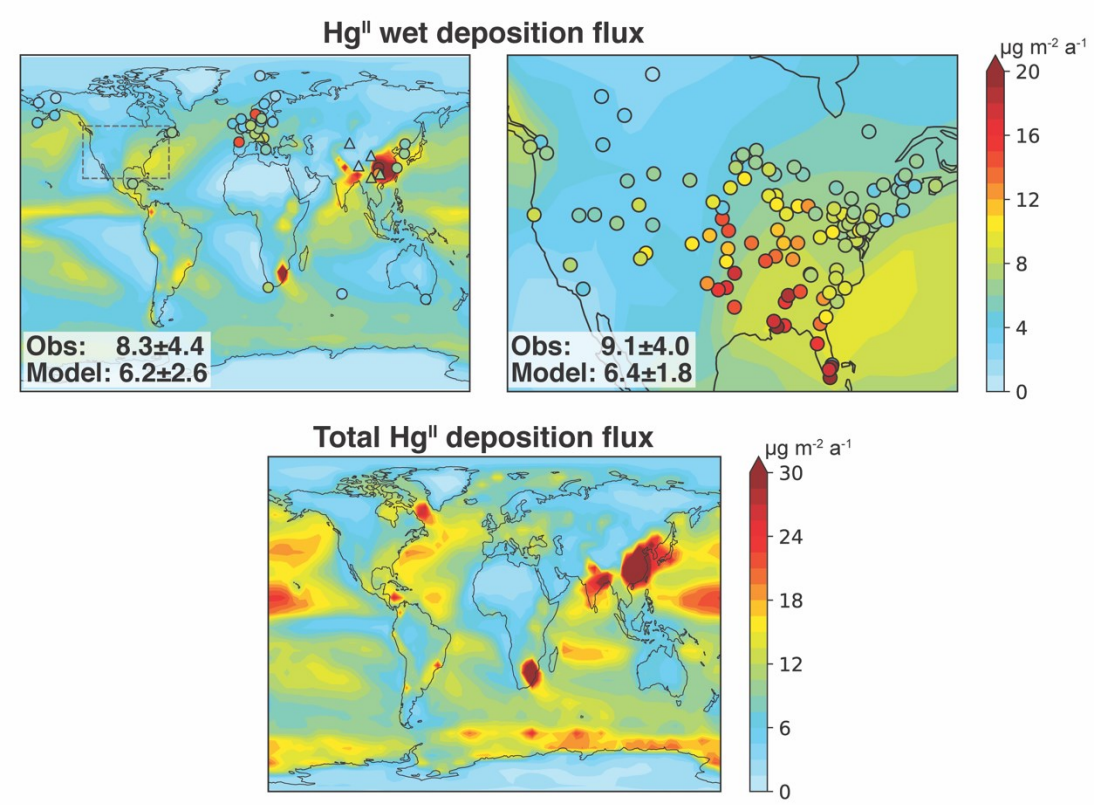


574
575 **Figure 4. Annual mean (2013–2015) $Hg^{II}$ deposition fluxes in GEOS-Chem. The top panels**
576 **show $Hg^{II}$ wet deposition fluxes overlaid by observations (filled circles and triangles)**
577 **compiled by Travnikov et al.[51] (courtesy of Hélène Angot), Sprovieri et al.,[114]**
578 **AMAP/UNEP,[113] and Fu et al.[115] Filled triangles represent high altitude sites. We only**
579 **include observations collected between 2010 and 2015. Values inset are the means ±**
580 **standard deviations for the global ensemble of sites (left panel) and for the subset of sites**
581 **over the contiguous US and Canada (right panel). The bottom panel shows total (wet + dry)**
582 **$Hg^{II}$ deposition fluxes.**

583 **TOC art:**

584

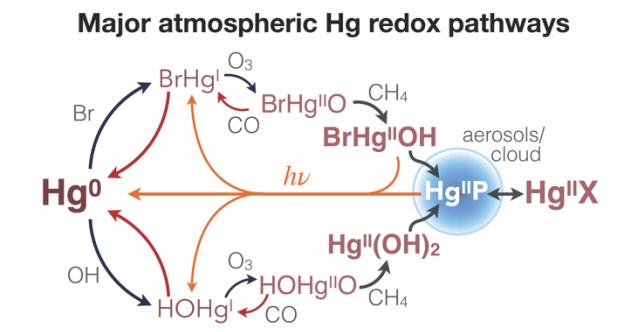


585

586

587 For Table of Contents only